

A Flexible Solid Composite Electrolyte with Vertically Aligned and Connected Ion-Conducting Nanoparticles for Lithium Batteries

Haowei Zhai,[†] Pengyu Xu,[†] Mingqiang Ning,^{†,‡} Qian Cheng,[†] Jyotirmoy Mandal,[†] and Yuan Yang^{*,†}

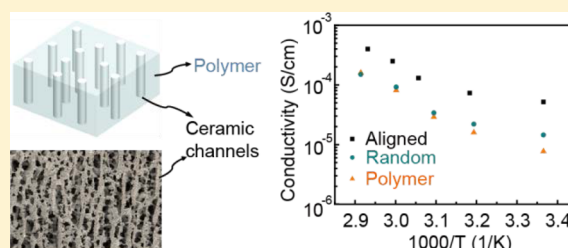
[†]Program of Materials Science and Engineering, Department of Applied Physics and Applied Mathematics, Columbia University, New York, New York 10025, United States

[‡]School of Materials Science & Engineering, Beijing Institute of Technology, Beijing, 100081, China

S Supporting Information

ABSTRACT: Replacing flammable organic liquid electrolytes with solid Li-ion conductors is a promising approach to realize safe rechargeable batteries with high energy density. Composite solid electrolytes, which are comprised of a polymer matrix with ceramic Li-ion conductors dispersed inside, are attractive, since they combine the flexibility of polymer electrolytes and high ionic conductivities of ceramic electrolytes. However, the high conductivity of ceramic fillers is largely compromised by the low conductivity of the matrix, especially when nanoparticles (NPs) are used. Therefore, optimizations of the geometry of ceramic fillers are critical to further enhance the conductivity of composite electrolytes. Here we report the vertically aligned and connected $\text{Li}_{1+x}\text{Al}_x\text{Ti}_{2-x}(\text{PO}_4)_3$ (LATP) NPs in the poly(ethylene oxide) (PEO) matrix to maximize the ionic conduction, while maintaining the flexibility of the composite. This vertically aligned structure can be fabricated by an ice-templating-based method, and its conductivity reaches 0.52×10^{-4} S/cm, which is 3.6 times that of the composite electrolyte with randomly dispersed LATP NPs. The composite electrolyte also shows enhanced thermal and electrochemical stability compared to the pure PEO electrolyte. This method opens a new approach to optimize ion conduction in composite solid electrolytes for next-generation rechargeable batteries.

KEYWORDS: Ice templating, solid electrolyte, vertically aligned structure, energy storage



Lithium-based rechargeable batteries are important energy storage devices for portable electronics, electric vehicles, and grid-level energy storage.^{1,2} High energy density, high safety, and low cost are the essential factors for developing next-generation lithium batteries. State-of-the-art Li-ion batteries (LIBs) use organic liquid-based electrolytes, which readily conduct ions and have a reasonably large stability window of ~4 V, leading to both high power and high energy densities.^{1–3} However, the organic liquid electrolytes have several drawbacks, such as high flammability, side reactions with both anode and cathode, electrolyte decomposition at high temperatures, potential leakage, and toxicity.^{3–5} Solid electrolytes are attractive compared to liquid organic electrolytes, as they are much less flammable and less reactive with electrode materials.^{6–9} Moreover, they can also suppress the growth of dendrites in lithium anode, which has a specific capacity ten times that of graphite anode, and the most negative electrode potential (–3.04 V vs standard hydrogen electrode). Therefore, the successful development of solid electrolytes could potentially lead to rechargeable batteries with high safety, high energy density, and low cost.

Solid polymer electrolytes and inorganic ceramic electrolytes are most widely studied among solid electrolytes. Solid polymer electrolytes typically use poly(ethylene oxide) (PEO) as the matrix with lithium salts (e.g., LiClO_4) filled inside,^{1,10,11} while ceramic electrolytes are commonly based on oxides^{12,13} and

sulfides.^{14,15} High ionic conductivities of 10^{-4} – 10^{-2} S/cm have been observed in various ceramic electrolytes, such as NaSICON-type $\text{Li}_{1+x}\text{Al}_x\text{Ti}_{2-x}(\text{PO}_4)_3$ (LATP),^{16–18} garnet-type $\text{Li}_7\text{La}_3\text{Zr}_2\text{O}_{12}$ (LLZO),^{12,19,20} and sulfides.^{14,15} However, ceramics are typically rigid, difficult to process, and exhibit high interfacial resistance with electrode materials.^{21,22} In contrast, solid polymer electrolytes can be prepared by simple solution-based processes, but they typically have low ionic conductivities ($<10^{-5}$ S/cm at room temperature).^{11,23,24}

To combine the advantages of both types of electrolytes, composite electrolytes have been developed where ceramic particles are dispersed in a polymer electrolyte matrix (Figure 1a).²⁵ As demonstrated in previous work, the fillers could be either non- Li^+ conducting, such as Al_2O_3 ,²⁶ SiO_2 ,¹¹ TiO_2 ,²⁷ and ZrO_2 ,²⁸ or Li^+ conducting, such as $\text{Li}_{0.5}\text{La}_{0.5}\text{TiO}_3$ (LLTO),²⁹ LLZO,³⁰ and LATP.^{31,32} For nonconducting fillers, ionic conductivities in the order of 10^{-5} S/cm can be achieved, and the mechanism is considered to be the amorphization of PEO and the creation of space-charge regions to facilitate Li^+ transport.^{11,33} For ion-conducting fillers, the ionic conductivity in the order of 10^{-4} S/cm has been reported.²⁵ However, the arrangement of fillers is either uniform dispersion¹¹ or fibers

Received: February 17, 2017

Revised: April 11, 2017

Published: April 14, 2017

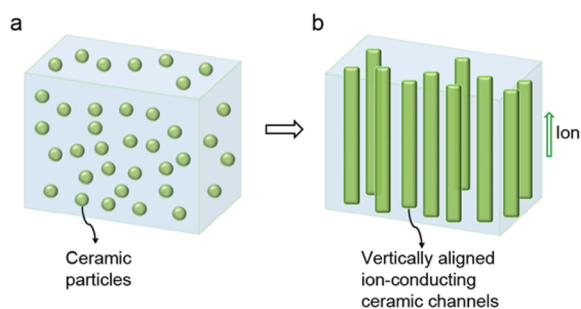


Figure 1. Schematic of vertically aligned and connected ceramic channels for enhancing ionic conduction. (a) Ceramic particles are randomly dispersed in the polymer matrix, where ion transport is blocked by the polymer matrix with a low conductivity. (b) Vertically aligned and connected structure to facilitate ion transport, which can be realized by the ice-templating method.

nearly in parallel to the surface of the solid electrolyte membrane.²⁵ For uniform dispersions, ion transport is significantly obstructed by the PEO matrix with a low conductivity, and conductivities even lower than the polymer matrix itself may be observed.³³ For fibers, a significant portion of ceramic do not contribute to ion conduction as they are aligned in parallel to the electrolyte surface. To maximize the ionic conductivity of the composite electrolyte, it is ideal to have vertically aligned and connected ceramic conductors which is also predicted in a recent review article,³⁴ as shown in Figure 1b. Here we present an ice-templating-based method to fabricate such structures in a composite electrolyte, where vertically aligned ion-conductive ceramic fillers form fast pathways for Li^+ transport, while the polymer matrix provides flexibility and mechanical support of the composite. In this

work, LATP filler in PEO is used as an example. The composite electrolyte reaches an ionic conductivity of 0.52×10^{-4} S/cm, which is close to the theoretical value based on the conductivity and volume portion of LATP (0.45×10^{-4} S/cm). The conductivity is largely limited by that of the ceramic phase, but this method can be extended to other ceramic systems, such as LLZO and even sulfides, to further enhance the ionic conductivity.

Figure 2a illustrates the principle of the ice-templating process, which has been developed in the past decade to form vertical structures for thermal insulation, battery electrodes, and other functional materials.^{35–42} In our experiments, the LATP nanoparticles (NPs) are dispersed in water and cast onto a substrate (step 1), after which the bottom end is slowly cooled. Therefore, a vertical temperature gradient forms, and ice nucleates from the bottom of the suspension, pushing the ceramic particles together to form vertically aligned structures (step 2). After ice sublimation, LATP particles are sintered together to form vertically aligned, straight channels for fast ionic transport (step 3 and 4). Lastly PEO/ LiClO_4 polymer electrolyte is filled into the porous ceramic structure to provide mechanical strength and flexibility (step 5).

To realize such a composite electrolyte with a rationally designed structure, LATP NPs with high ionic conductivity are needed. Such NPs are synthesized by a coprecipitation process⁴³ (see Supporting Information, SI, for details). The LATP NPs have an average size of 200–500 nm (Figure S1a), and pellets fabricated from the NPs show a reasonably high conductivity of 1.0×10^{-4} S/cm at room temperature, which is comparable with results in literature (Figure S1c).^{13,43–45} After synthesizing LATP NPs with a high conductivity, they are dispersed in deionized (DI) water to form a suspension.

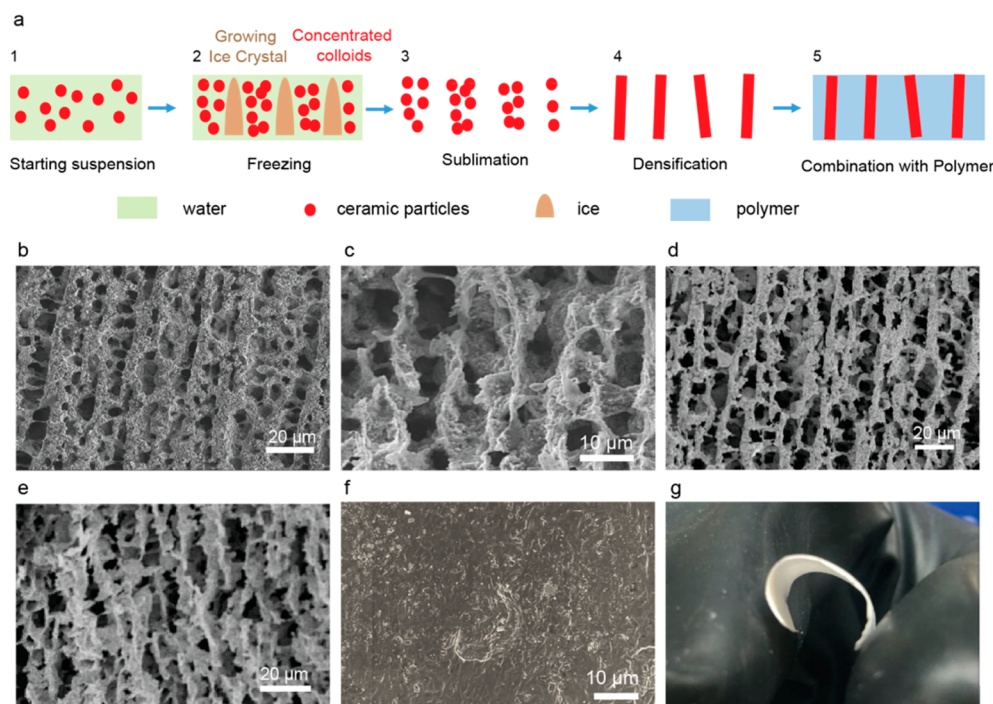


Figure 2. Ice-templating process and the as-fabricated composite electrolyte. (a) 1. Starting suspension with ceramic particles dispersed in water. 2. Unidirectional freezing through cooling from the bottom. 3. Sublimation of ice in a vacuum. 4. Densification of ceramics through sintering. 5. Combination with the polymer electrolyte matrix to form the composite electrolyte. (b–e) SEM images of the ice-templated LATP channels. (b) Top view before sintering, (c) cross-section view before sintering, (d) top view after sintering, and (e) cross-section view after sintering. (f) SEM image (top view) of the aligned structure after filling the PEO/ LiClO_4 electrolyte. (g) Camera image showing the flexibility of the composite film.

Poly(vinyl alcohol) (PVA) and polyethylene glycol (PEG, MW = 400) are added as a binder and plasticizer, respectively. Then the suspension is dropped onto an Al_2O_3 plate, which is cooled afterward from the bottom by a thermoelectric plate with a cooling rate of $3\text{ }^\circ\text{C}/\text{min}$. After the water is fully frozen, a vacuum is applied to sublime ice, and the vertically aligned structure of LAMP particles are revealed (see SI for details). Figure 2b and c are the SEM images of the top and cross-section views of the vertically aligned ice-templated LAMP structure before sintering, respectively. Clearly, straight pores are formed over a large area with typical pore sizes of 5–10 μm . After sintering, the vertically aligned porous structure still remains, and particles are better sintered together, providing the direct pathways for lithium ion transport (Figure 2d and e). From SEM images, the typical film thickness is measured to be $\sim 100\text{ }\mu\text{m}$ and can be further reduced by lowering the thickness of the initial suspension coating. After sintering the LAMP NPs and adding the PEO polymer electrolyte, the LAMP porous structure is fully covered by PEO/ LiClO_4 (Figure 2f). The composite electrolyte is also flexible and can be easily bent (Figure 2g).

To validate our assumption that the vertically aligned and connected channels could enhance the ionic conductivity of the composite electrolyte, electrochemical impedance spectroscopy (EIS) measurements of three types of samples at different temperatures are taken: a pure PEO electrolyte, PEO with randomly dispersed LAMP NPs, and PEO with ice-templated LAMP NPs (Figure 3a). In all samples, the molar ratio of ethylene oxide (EO) to LiClO_4 is fixed at 8:1. The volume percentages of the LAMP NPs in the two composite electrolytes are both 40% based on the thermogravimetric analysis. Since

the surface of ice-templated LAMP NPs + polymer composite is rough, it is difficult to get accurate EIS results with either stainless steel or sputtered Au electrode. Therefore, lithium metal foils are used as electrodes for EIS measurement in all samples, and thus two semicircles are observed, which correspond to the resistance of bulk electrolyte and the geometric capacitance in parallel (high frequencies), and the charge transfer resistance and the double layer capacitance in parallel (low frequencies), respectively. To extract the electrolyte conductivity, an equivalent circuit shown in Figure 3a is used to fit the two semicircles in the plot, and the fitting results are illustrated as red curves. The conductivity of pure PEO electrolyte is only $3.6 \times 10^{-8}\text{ S/cm}$ at room temperature (see Table 1 for conductivities at room temperature), and it

Table 1. Conductivities for Different Structures at Room Temperature, Without and with the Plasticizer PEG

filler matrix	no filler (S/cm)	randomly dispersed LAMP NPs (S/cm)	ice-templated LAMP NPs (S/cm)
PEO	3.6×10^{-8}	1.4×10^{-6}	6.8×10^{-6}
PEO/PEG	7.7×10^{-6}	1.5×10^{-5}	5.2×10^{-5}

increases to $7.0 \times 10^{-5}\text{ S/cm}$ at $70\text{ }^\circ\text{C}$, which is consistent with previous reports.^{11,46} After adding the randomly dispersed LAMP NPs, the conductivity increases to $1.4 \times 10^{-6}\text{ S/cm}$ at room temperature. The increased conductivity is quite small compared to the conductivity of LAMP itself ($\sim 1.0 \times 10^{-4}\text{ S/cm}$), as the LAMP NPs are not connected and the conduction of Li^+ ions is limited by the low conductivity of the matrix. The ionic conductivity of the ice-templated LAMP film reaches $6.8 \times 10^{-6}\text{ S/cm}$ at room temperature, five times that of the randomly dispersed case. This shows that this design of vertically aligned and connected LAMP fillers indeed improves the conductivity significantly. To make fair comparison between the results with lithium electrodes and the results with stainless steel electrodes, we also perform EIS measurements on the pure PEO electrolyte with stainless steel electrodes, which gives consistent results with lithium metal electrodes (Figure S3).

Although an improved ionic conductivity has been observed in the ice-templated composite electrolyte, it is still much less than the theoretical value ($0.4 \times 10^{-4}\text{ S/cm}$) based on the volume portion and the ionic conductivity of LAMP (40%, $1.0 \times 10^{-4}\text{ S/cm}$) and PEO (60%, $3.6 \times 10^{-8}\text{ S/cm}$). This is likely due to the poor ionic transport at particle–particle interfaces, which may arise from two factors: (1) the poor conduction at the LAMP–LAMP particle interfaces, since the ice-templated film is not pressed, and (2) interfacial regions which form at the LAMP/PEO interfaces and block the transport of Li ions along the pathways of LAMP–PEO–LAMP.^{33,47} To address this issue, PEG is added (see SI for details) into the composite as a plasticizer to reduce the interfacial resistance and thus enhance the ionic conductivity. Although PEG is not stable with the lithium metal in the long term, here it is used as a model example to demonstrate the enhancement of the ionic conductivity after improving the interfacial conduction. As done for to EIS tests without PEG, three kinds of samples are prepared, including the pure PEO/PEG electrolyte, the PEO/PEG electrolyte with randomly dispersed LAMP NPs, and the PEO/PEG electrolyte with ice-templated LAMP NPs. As earlier, the volume portion of LAMP NPs is kept at 40% in the two composite electrolytes. The pure PEO/PEG electrolyte has a

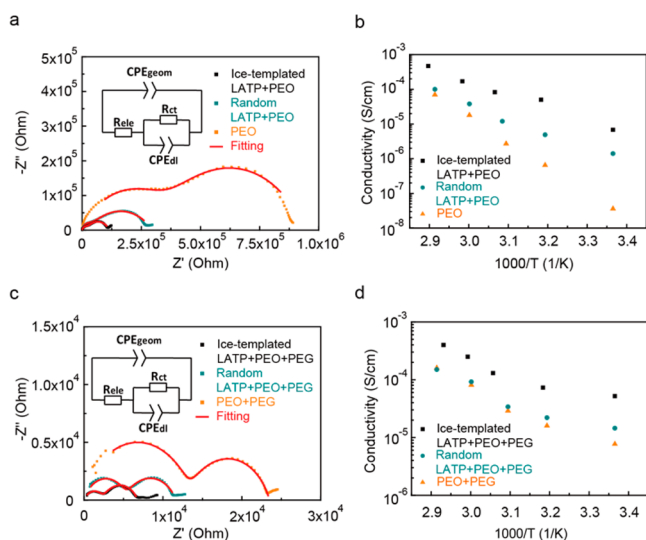


Figure 3. (a) EIS at room temperature for the pure PEO, PEO/randomly dispersed LAMP NPs, and PEO/ice-templated LAMP NPs electrolytes. The inset is the corresponding equivalent circuit. (b) Ionic conductivities of the three structures in panel a at different temperatures. (c) EIS at room temperature for the pure PEO/PEG, PEO/PEG/randomly dispersed LAMP NPs, and PEO/PEG/ice-templated LAMP NPs electrolytes. The inset is the equivalent circuit. (d) Ionic conductivities of the three structures in panel c at different temperatures. In panels a and c, R_{ct} and CPE_{dl} represent the charge transfer resistance and the double layer capacitance; R_{ele} and CPE_{geom} indicate the resistance of the electrolyte and the geometric capacitance. Magnified images of panels a and c are shown in Figure S4.

conductivity of 7.7×10^{-6} S/cm at room temperature, which is 2 orders of magnitude higher than that of the pure PEO electrolyte. The conductivity further increases to 1.6×10^{-4} S/cm at 70 °C. After adding the randomly dispersed LAMP NPs, the conductivity is 1.5×10^{-5} S/cm at room temperature, which is only twice that of the pure PEO/PEG electrolyte. This suggests that LAMP does not help improve the ion transport significantly if particles are not well-connected, especially when the matrix has a high conductivity. In contrast, the ice-templated LAMP film reaches a conductivity of 0.52×10^{-4} S/cm at room temperature, 3.6 times that of the PEO/PEG electrolyte with randomly dispersed LAMP NPs. The value is also 6.8 times that of the pure PEO/PEG electrolyte (Figure 3c). These results demonstrate that the rational design of vertically aligned LAMP fillers play a role for the conductivity increase as well in the composite with the PEG plasticizer. Moreover, the conductivity of the PEO/PEG/ice-templated LAMP composite electrolyte (0.52×10^{-4} S/cm) is 7.6 times that of the one without PEG (6.8×10^{-6} S/cm), indicating the plasticizer indeed improve transport at the LAMP/LAMP and LAMP/PEO interfaces. The conductivity of PEO/PEG/ice-templated LAMP composite electrolyte (0.52×10^{-4} S/cm) is also almost the same as the theoretical value of conductivity (0.45×10^{-4} S/cm) discussed above, which supports the effectiveness of the ice-templated structure. This also suggests that a higher conductivity of 3.0×10^{-4} S/cm could be realized if ceramic fillers with higher conductivity are used, such as LLZO^{12,19,20} or sulfides.^{14,15} The reason why the conductivity is beyond the theoretical value may be that the PEG plasticizer helps improve the interfacial transport between ceramic particles and polymer/ceramic particles.

The porous LAMP film itself without polymer is too fragile to measure its intrinsic conductivity. To validate that LAMP contributes significantly to the ionic conduction, we measured the conductivity of the sintered porous LAMP film soaked in dilute liquid organic electrolyte (0.125 mM LiPF₆ in ethylene carbonate/diethyl carbonate of weight ratio 1:1, with the conductivity of 1.1×10^{-5} S/cm) instead of polymer. Such a sample shows a conductivity of 5.9×10^{-5} S/cm (Figure S5). Based on the porosity (60%) of the film and the fact that the liquid electrolyte and LAMP are in parallel, the corresponding conductivity of the LAMP bulk phase is estimated to be 1.2×10^{-4} S/cm, which is consistent with our result of the LAMP pellet conductivity in SI (Figure S1). This indicates that the LAMP phase is the key reason for the high conductivity.

Thermogravimetric analysis (TGA) is used to understand the thermal stability of the composite electrolyte. The electrolyte is heated in O₂ with a heating rate of 10 °C/min. Both the pure PEO/PEG and PEO/PEG/ice-templated LAMP composite samples are tested. The pure PEO/PEG electrolyte is thermally stable at up to temperatures of around 145 °C, whereas the ice-templated composite is stable up to around 167 °C, indicating that LAMP helps improve the thermal stability of the composite electrolyte. Above this temperature, polymers begin to decompose, and most mass is lost before 400 °C. For the ice-templated composite electrolyte, the weight loss occurs in the similar temperature range, and the mass left is from LAMP NPs inside the composite electrolyte. The ice-templated LAMP fillers also stabilize the structure of the composite solid electrolyte. In Figure 4b, without any ice-templated structure, the PEO/PEG electrolyte melts and shrinks after heating at 180 °C for 30 min since there is no rigid ceramic backbone inside. In contrast, the electrolyte with ice-templated LAMP NPs is

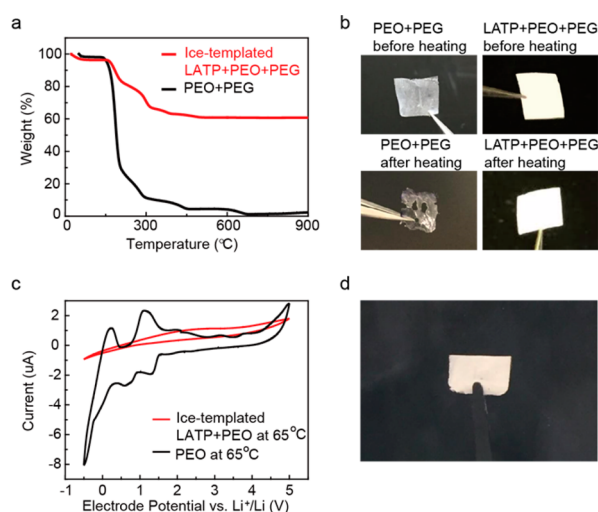


Figure 4. (a) TGA curves of the PEO/PEG and PEO/PEG/ice-templated LAMP electrolytes. The heating rate is 10 °C/min in O₂ environment. (b) PEO/PEG and PEO/PEG/ice-templated LAMP electrolytes before and after heating at 180 °C for 30 min. (c) Cyclic voltammetry of the pure PEO and PEO/ice-templated LAMP NPs electrolytes at 65 °C. (d) Image of the ice-templated LAMP composite after 24 h in contact with Li metal.

intact at 180 °C, showing that the ceramic fillers can effectively stabilize the integrity of the structure.

To understand how the ice-templated structure affects the stability of the composite electrolyte, cyclic voltammetry is carried out at 65 °C for both the pure PEO electrolyte and that with ice-templated LAMP NPs inside (Figure 4c). For the pure PEO case, reduction peaks are observed at 0.7 and 1.3 V vs Li⁺/Li, which may be a result of reduction of PEO and LiClO₄.⁴⁸ In contrast, the ice-templated sample is more stable at both low and high potentials vs Li⁺/Li. The possible reason is that LAMP helps stabilize PEO in the bulk region, leading to a better electrochemical stability. The electrochemical behavior of pure LAMP, such as cyclic voltammetry and galvanostatic tests, is discussed in the SI (Figure S6). The conjecture on the stability of the PEO/LAMP composite electrolyte is also supported by the results of direct contact between the lithium metal and the PEO/ice-templated LAMP NPs. After 24 h of contact with lithium metal, the film remains white (Figure 4d), indicating that there is no reaction between lithium metal and LAMP, whereas an LAMP pellet in contact with lithium metal turns into black after 24 h (Figure S7).

To evaluate the flexibility of the composite electrolyte, the ice-templated LAMP/PEO/PEG composite film is bent for various times, followed by measurement of ionic conductivity (Figure 5a). The film is first bent down to diameter of 5 cm up to 100 times. After an initial drop, the conductivity becomes stable after bending for 5 times. After 100 times bending, the conductivity remains at 82% of the initial value. The composite film is also bent down to diameter of 2.5 cm for various times. After 100 times, the conductivity remains at 74% of that before bending. These data supports that as-prepared composite film with vertical structure is mechanically flexible.

The modulus of the composite electrolyte is also studied. Standard stress/strain curves are measured for both tension and compression. The tensile tests are conducted along the in-plane direction with a model 5948 MicroTester Instron instrument, and the film shows the standard linear strain–stress curve at low strains (Figure 5b), which is used to calculate Young's

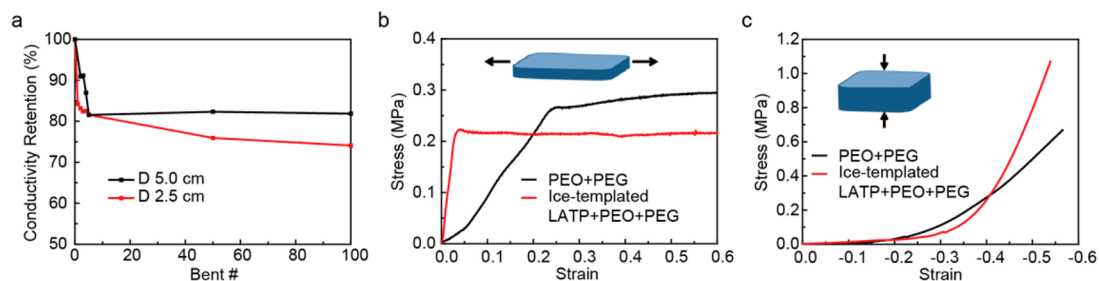


Figure 5. Mechanical properties of as-prepared composite electrolyte. (a) Ionic conductivity vs bending times. After an initial drop, the PEO/PEG/ice-templated LAMP film shows stable ionic conductivities. (b) Tensile stress/strain curves for PEO/PEG and PEO/PEG/ice-templated LAMP samples. The inset is the schematic of the in-plane tensile test. (c) Compressive stress/strain curves for PEO/PEG and PEO/PEG/ice-templated LAMP samples. The inset is the schematic of the compressive test along the *z* direction.

modulus. For the compressive tests, multiple pieces of composite electrolyte film are first compressed at 500 MPa to form a pellet. Then the pellet is compressed by the same MicroTester above. Nonlinear behavior is observed in compression. The initial low modulus region is likely due to the stacking of multiple pieces. Therefore, the compression modulus is measured based on the linear regimes at larger strain (0.35–0.55 for PEO/PEG and 0.40–0.53 for PEO/PEG/ice-templated LAMP). For PEO/PEG samples, moduli are 1.9 and 1.4 MPa for tension and compression, respectively. For PEO/PEG/ice-templated LAMP films, moduli are 6.6 and 3.6 MPa for tension and compression, respectively. Obviously the incorporation of LAMP ceramic particles enhances the Young's modulus of the solid electrolyte. The measured values are consistent with various previous reports on polymer electrolytes.^{49,50} The work by Khurana et al. shows that even lower modulus is capable of suppressing dendrite growth.⁵¹ Experimental details can be found in the SI.

This report uses LAMP as an example to demonstrate the effectiveness of vertically aligned and connected ceramic fillers for enhancing ionic conductivity, and the concept can be applied to other ceramic solid electrolytes such as LLZO and sulfides. LLZO is known to be unstable in water due to the ion-exchange between LLZO and protons in water.⁵² However, we find that adding LiOH into water could compensate lithium loss in water and the LLZO phase is recovered after sintering at 900 °C (Figure S8). Therefore, LLZO is compatible with proposed ice-templating method. For sulfides, water can be replaced by camphene, which also produces the vertical structure and allows the operation at room temperature.⁵³

In summary, a flexible solid composite electrolyte with vertically aligned and connected LAMP NPs is prepared by ice-templating process. The aligned structure provides direct channels for lithium ions transport and improves the ionic conductivity significantly. The flexible solid-state electrolyte exhibits an ionic conductivity of 0.52×10^{-4} S/cm at room temperature, 3.6 times that of the PEO electrolyte with randomly dispersed LAMP NPs inside. The value is also similar to the theoretical prediction (0.45×10^{-4} S/cm) due to the improvement of the interfaces between LAMP particles and polymer/LAMP particles. The composite electrolyte also shows a high geometric stability at 180 °C and better electrochemical stability than the pure polymer electrolyte. This approach can be applied to other ceramic systems, such as LLZO and sulfides, to further enhance the ionic conductivity.

■ ASSOCIATED CONTENT

📄 Supporting Information

The Supporting Information is available free of charge on the ACS Publications website at DOI: 10.1021/acs.nanolett.7b00715.

Synthesis process and properties of LAMP. Ice-templating process setup. Preparation process of polymer and composite electrolytes. EIS results with different electrodes. Magnified images of Figure 3. EIS for ice-templated LAMP with liquid electrolyte. Cyclic voltammetry and charge/discharge measurements for pure LAMP. LAMP pellet in contact with lithium metal for 24 h. Mechanical tests for the composite films. XRD of LLZO powder soaked in pure H₂O and 2 M LiOH solution (PDF)

■ AUTHOR INFORMATION

✉ Corresponding Author

*E-mail: yy2664@columbia.edu.

ORCID

Haowei Zhai: 0000-0002-7030-3563

Author Contributions

H.Z., P.X., and M.N. contributed equally to this paper.

Notes

The authors declare no competing financial interest.

■ ACKNOWLEDGMENTS

Y.Y. acknowledges support from startup funding by Columbia University and seed funding from Lenfest Center of Sustainable Energy at Columbia University. This work is supported by the NSF MRSEC program through Columbia in the Center for Precision Assembly of Superstratic and Superatomic Solids (DMR-1420634). We would like to acknowledge support from Kristin Myers and Charles Jayyosi in Department of Mechanical Engineering at Columbia University on mechanical measurement.

■ REFERENCES

- (1) Tarascon, J. M.; Armand, M. *Nature* **2001**, *414*, 359–367.
- (2) Whittingham, M. S. *MRS Bull.* **2008**, *33*, 411–419.
- (3) Xu, K. *Chem. Rev.* **2004**, *104*, 4303–4417.
- (4) Armand, M.; Endres, F.; MacFarlane, D. R.; Ohno, H.; Scrosati, B. *Nat. Mater.* **2009**, *8*, 621–629.
- (5) Goodenough, J. B.; Park, K. S. *J. Am. Chem. Soc.* **2013**, *135*, 1167–1176.
- (6) Wu, H.; Chan, G.; Choi, J. W.; Ryu, I.; Yao, Y.; McDowell, M. T.; Lee, S. W.; Jackson, A.; Yang, Y.; Hu, L.; Cui, Y. *Nat. Nanotechnol.* **2012**, *7*, 310–315.

- (7) Kim, J. G.; Son, B.; Mukherjee, S.; Schuppert, N.; Bates, A.; Kwon, O.; Choi, M. J.; Chung, H. Y.; Park, S. *J. Power Sources* **2015**, *282*, 299–322.
- (8) Sun, Y. G. *Nano Energy* **2013**, *2*, 801–816.
- (9) Verma, P.; Maire, P.; Novák, P. *Electrochim. Acta* **2010**, *55*, 6332–6341.
- (10) Scrosati, B.; Hassoun, J.; Sun, Y.-K. *Energy Environ. Sci.* **2011**, *4*, 3287–3295.
- (11) Lin, D.; Liu, W.; Liu, Y.; Lee, H. R.; Hsu, P.-C.; Liu, K.; Cui, Y. *Nano Lett.* **2016**, *16*, 459–465.
- (12) Buschmann, H.; Dolle, J.; Berendts, S.; Kuhn, A.; Bottke, P.; Wilkening, M.; Heitjans, P.; Senyshyn, A.; Ehrenberg, H.; Lotnyk, A.; Duppel, V.; Kienle, L.; Janek, J. *Phys. Chem. Chem. Phys.* **2011**, *13*, 19378–19392.
- (13) Liu, X.; Fu, J.; Zhang, C. *Nanoscale Res. Lett.* **2016**, *11*, 551.
- (14) Fergus, J. W. *J. Power Sources* **2010**, *195*, 4554–4569.
- (15) Suo, L.; Hu, Y.-S.; Li, H.; Armand, M.; Chen, L. *Nat. Commun.* **2013**, *4*, 1481.
- (16) Hasegawa, S.; Imanishi, N.; Zhang, T.; Xie, J.; Hirano, A.; Takeda, Y.; Yamamoto, O. *J. Power Sources* **2009**, *189*, 371–377.
- (17) Knauth, P. *Solid State Ionics* **2009**, *180*, 911–916.
- (18) Imanishi, N.; Hasegawa, S.; Zhang, T.; Hirano, A.; Takeda, Y.; Yamamoto, O. *J. Power Sources* **2008**, *185*, 1392–1397.
- (19) Ohta, S.; Kobayashi, T.; Seki, J.; Asaoka, T. *J. Power Sources* **2012**, *202*, 332–335.
- (20) Kokal, I.; Somer, M.; Notten, P. H. L.; Hintzen, H. T. *Solid State Ionics* **2011**, *185*, 42–46.
- (21) Lim, Y. J.; Kim, H. W.; Lee, S. S.; Kim, H. J.; Kim, J.-K.; Jung, Y.-G.; Kim, Y. *ChemPlusChem* **2015**, *80*, 1100–1103.
- (22) Ohta, N.; Takada, K.; Zhang, L.; Ma, R.; Osada, M.; Sasaki, T. *Adv. Mater.* **2006**, *18*, 2226–2229.
- (23) Scrosati, B.; Garche, J. *J. Power Sources* **2010**, *195*, 2419–2430.
- (24) Manuel Stephan, A.; Nahm, K. S. *Polymer* **2006**, *47*, 5952–5964.
- (25) Fu, K.; Gong, Y. H.; Dai, J. Q.; Gong, A.; Han, X. G.; Yao, Y. G.; Wang, C. W.; Wang, Y. B.; Chen, Y. N.; Yan, C. Y.; Li, Y. J.; Wachsmann, E. D.; Hu, L. B. *Proc. Natl. Acad. Sci. U. S. A.* **2016**, *113*, 7094–7099.
- (26) Yang, C.-M.; Kim, H.-S.; Na, B.-K.; Kum, K.-S.; Cho, B. W. *J. Power Sources* **2006**, *156*, 574–580.
- (27) Liu, Y.; Lee, J. Y.; Hong, L. *J. Appl. Polym. Sci.* **2003**, *89*, 2815–2822.
- (28) Croce, F.; Sacchetti, S.; Scrosati, B. *J. Power Sources* **2006**, *162*, 685–689.
- (29) Liu, W.; Sun, J.; Hsu, P.-C.; Li, Y.; Lee, H.-W.; Cui, Y. *Nano Lett.* **2015**, *15*, 2740–2745.
- (30) Langer, F.; Bardenhagen, L.; Glenneberg, J.; Kun, R. *Solid State Ionics* **2016**, *291*, 8–13.
- (31) Liu, W.; Milcarek, R. J.; Falkenstein-Smith, R. L.; Ahn, J. *J. Electrochem. Energy Convers. Storage* **2016**, *13*, 021008–021008–6.
- (32) Wang, Y.-J.; Pan, Y.; Chen, L. *Mater. Chem. Phys.* **2005**, *92*, 354–360.
- (33) Dudney, N.; Kalnaus, S. https://energy.gov/sites/prod/files/2015/06/f23/es182_dudney_2015_o.pdf (accessed Sept 26, 2016).
- (34) Lin, D.; Liu, Y.; Cui, Y. *Nat. Nanotechnol.* **2017**, *12*, 194–206.
- (35) Wicklein, B.; Kocjan, A.; Salazar-Alvarez, G.; Carosio, F.; Camino, G.; Antonietti, M.; Bergström, L. *Nat. Nanotechnol.* **2014**, *10*, 277–283.
- (36) Sander, J. S.; Erb, R. M.; Li, L.; Gurijala, A.; Chiang, Y. M. *Nat. Energy* **2016**, *1*, 16099.
- (37) Deville, S.; Saiz, E.; Nalla, R. K.; Tomsia, A. P. *Science* **2006**, *311*, 515–518.
- (38) Deville, S. *Adv. Eng. Mater.* **2008**, *10*, 155–169.
- (39) Pawelec, K. M.; Husmann, A.; Best, S. M.; Cameron, R. E. *Appl. Phys. Rev.* **2014**, *1*, 021301.
- (40) Deville, S. *J. Mater. Res.* **2013**, *28*, 2202–2219.
- (41) Kawahara, H. *J. Biosci. Bioeng.* **2002**, *94*, 492–496.
- (42) Gutierrez, M. C.; Ferrer, M. L.; del Monte, F. *Chem. Mater.* **2008**, *20*, 634–648.
- (43) Duluard, S.; Paillassa, A.; Puech, L.; Vinatier, P.; Turq, V.; Rozier, P.; Lenormand, P.; Taberna, P. L.; Simon, P.; Ansart, F. *J. Eur. Ceram. Soc.* **2013**, *33*, 1145–1153.
- (44) Best, A. S.; Forsyth, M.; MacFarlane, D. R. *Solid State Ionics* **2000**, *136–137*, 339–344.
- (45) Mariappan, C. R.; Gellert, M.; Yada, C.; Rosciano, F.; Roling, B. *Electrochem. Commun.* **2012**, *14*, 25–28.
- (46) Croce, F.; Appetecchi, G. B.; Persi, L.; Scrosati, B. *Nature* **1998**, *394*, 456–458.
- (47) Zheng, J.; Tang, M.; Hu, Y.-Y. *Angew. Chem., Int. Ed.* **2016**, *55*, 12538–12542.
- (48) Shi, Q.; Xue, L.; Qin, D.; Du, B.; Wang, J.; Chen, L. *J. Mater. Chem. A* **2014**, *2*, 15952–15957.
- (49) Khan, M. S.; Sultana, S. *Int. J. Polym. Sci.* **2015**, *2015*, 10.
- (50) Tung, S.-O.; Ho, S.; Yang, M.; Zhang, R.; Kotov, N. A. *Nat. Commun.* **2015**, *6*, 6152.
- (51) Khurana, R.; Schaefer, J. L.; Archer, L. A.; Coates, G. W. *J. Am. Chem. Soc.* **2014**, *136*, 7395–7402.
- (52) Ma, C.; Rangasamy, E.; Liang, C.; Sakamoto, J.; More, K. L.; Chi, M. *Angew. Chem., Int. Ed.* **2015**, *54*, 129–133.
- (53) Hong, C.; Zhang, X.; Han, J.; Du, J.; Zhang, W. *Mater. Chem. Phys.* **2010**, *119*, 359–362.